
Disclaimer

This manuscript is under revision in NATURE COMMUNICATIONS EARTH & ENVIRONMENT, and is not peer-reviewed.

Please feel free to contact any of the authors with feedback and suggestions for improvements.

Document history

Date	Action
03/Aug/2022	MS sent to co-authors for final draft acceptance Supplementary materials uploaded to Zenodo MS Submitted to EarthArXiv MS Submitted to Communications Earth and Environment
03/Oct/2022	Decision received, Major revisions required
04/Mar/2023	Revised MS submitted to EarthArxiv New version of supplementary materials uploaded to Zenodo Revised MS submitted to Communications Earth and Environment

THE INFLUENCE OF REEF ISOSTASY, DYNAMIC TOPOGRAPHY, AND GLACIAL ISOSTATIC ADJUSTMENT ON THE LAST INTERGLACIAL SEA-LEVEL RECORD OF NORTHEASTERN AUSTRALIA.

PREPRINT, COMPILED MARCH 3, 2023

Alessio Rovere^{1,2*}, Tamara Pico³, Frederick Richards⁴, Michael J. O’Leary⁵, Jerry X. Mitrovica⁶, Ian D. Goodwin^{7,8},
Jacqueline Austermann⁹, and Konstantin Latychev⁶

¹Department of Environmental Sciences, Informatics and Statistics, Ca’ Foscari University of Venice, IT

²MARUM - Center for Marine Environmental Sciences, University of Bremen, DE Germany

³Earth & Planetary Sciences Department, UC Santa Cruz, Santa Cruz, USA

⁴Department of Earth Science & Engineering, Imperial College London, London, UK

⁵School of Earth Sciences, University of Western Australia Oceans Institute, Perth, AU

⁶Department of Earth and Planetary Sciences, Harvard University, Boston, USA

⁷Climalab, New South Wales, AU

⁸Climate Change Research Centre and Australian Centre for Excellence in Antarctic Science, University of New South Wales, AU

⁹Department of Earth and Environmental Sciences & Lamont-Doherty Earth Observatory, Columbia University, New York, USA

ABSTRACT

NOTE FOR THE READER: this is a preprint of a manuscript submitted to Nature Communications Earth & Environment. This manuscript has not been peer-reviewed. Understanding sea level during the warmest peak of the Last Interglacial (125,000 yrs ago; Marine Isotope Stage 5e) is important for assessing future ice-sheet dynamics in response to climate change, and relies on the measurement and interpretation of paleo sea-level indicators, corrected for post-depositional vertical land motions. The coasts and continental shelves of northeastern Australia (Queensland) preserve an extensive Last Interglacial record in the facies of coastal strandplains onland and fossil reefs offshore. However, there is a discrepancy, amounting to tens of meters, in the elevation of sea-level indicators between offshore and onshore sites. Here, we assess the influence of geophysical processes that may have changed the elevation of these sea-level indicators since the Last Interglacial. We modeled sea-level change due to: i) dynamic topography; ii) glacial isostatic adjustment, and iii) isostatic adjustment due to coral reef loading, which we term "reef isostasy". We find that these processes caused relative sea-level changes on the order of, respectively, 10 m, 5 m, and 0.3 m since the Last Interglacial. Of these geophysical processes, the dynamic topography predictions most closely match the tilting observed between onshore and offshore sea-level markers. However, these combined geophysical processes cannot explain the full amplitude of the observed discrepancy between these sea-level indicators.

Keywords Last Interglacial · Sea level changes · NE Australia · Great Barrier Reef

1 INTRODUCTION

2 Below the modern Great Barrier Reef (GBR) reef flats, coring
3 has typically encountered shallow-water Last Interglacial (LIG,
4 MIS 5e, 125 kyrs) reefs between depths of 5 and 20m. Strik-
5 ingly, along the Queensland and far northern New South Wales
6 coastline, LIG strandplains are identified at higher elevations
7 than offshore LIG reefs, with ridge/swale heights ranging from
8 +3 to +9m above modern sea level. [63, 33]. These onshore
9 features are not as precisely dated as the sea-level indicators
10 found within fossil reefs in cores, however they were also ar-
11 guably formed during the LIG. The higher elevations of these
12 coastal strandplains are roughly consistent with estimates for
13 peak LIG global mean sea level (GMSL). Such estimates are
14 consistently above modern mean sea level (0 m), albeit they vary
15 substantially depending on study sites analyzed and corrections
16 for vertical land motions applied to the proxy record (from 6 to
17 9 m 45, 8 m 23, and 1-5 m 24).

18 The most obvious explanation of the discrepancy between on-
19 shore and offshore LIG relative sea-level indicators in Northeast-
20 ern Australia is that these two areas are subject to differential

vertical land motions. When reconstructing past global mean sea
level (GMSL) from geological sea-level proxies, it is essential to
disentangle the components causing globally averaged sea-level
changes from other regional processes that may have caused ver-
tical displacement of past sea-level indicators [71, 75]. Among
these, the most relevant are glacial isostatic adjustment (GIA)
[25], tectonic deformation processes [56] and mantle dynamic
topography (DT) [5].

Crustal loading due to local processes can also cause the vertical
displacement of observed sea-level indicators through isostatic
adjustment. For example, sediment loading can cause regional
sea level to depart significantly from the global mean along
major deltaic systems [17, 70, 27, 70, 77, 26, 94]. Karst erosion
is another mechanism that induces isostatic adjustment, through
mass unloading, causing a net crustal uplift. This process is
active in the Plio-Pleistocene shoreline complexes in Florida that
were uplifted following isostatic response to the karstification
(leading to rock mass loss) of the landscape [15, 66, 1, 95]. To
date, estimates of peak LIG GMSL from tropical areas have
not accounted for the isostatic response to coral reef loading
over the last glacial cycle. This process arises because corals

21
22
23
24
25
26
27
28
29
30
31
32
33
34
35
36
37
38
39
40
41

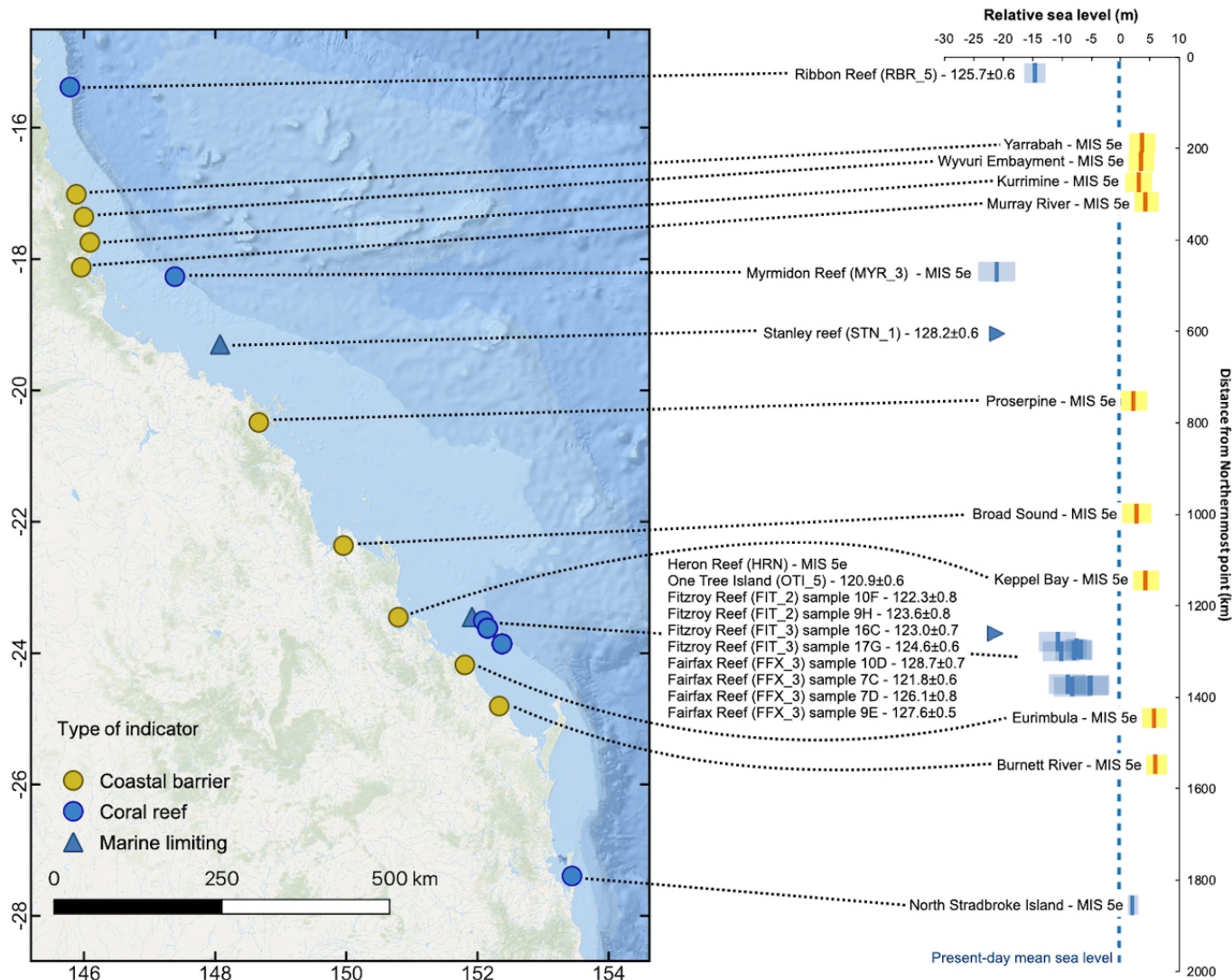


Figure 1: Map (left panel) and elevation plot (right panel) of LIG paleo RSL obtained from fossil reefs (blue markers) and beach barriers (yellow markers) along the GBR and the Queensland Coasts. Error bars represent 1-sigma ranges.

42 can grow into spatially extensive reefs, reaching thicknesses of
 43 several tens of meters during interglacials. The effect of reef
 44 accretion and related loading on local sea-level histories remains
 45 largely unexplored.

46 In this work, we model the influence of geophysical processes
 47 that may have changed the elevation of geologic sea-level indica-
 48 tors along the Queensland coasts and offshore, on the GBR,
 49 since the LIG. We assess the extent to which the combined
 50 geophysical processes of glacial isostatic adjustment and dyna-
 51 mic topography may have impacted the LIG sea-level record
 52 in this region. We also isolate the process of coral reef loading,
 53 and assess its contribution to regional departures from GMSL.
 54 While the combined geophysical processes modeled in this study
 55 cannot fully explain the amplitude of the observed discrepancy
 56 between onshore and offshore sea-level markers in the study
 57 area, we find that dynamic topography contributes the largest
 58 magnitude to the observed tilting.

1 LIG SEA-LEVEL INDICATORS

The study of past sea-level changes relies on the measurement
 and dating of relative sea-level (RSL) indicators, i.e. geological
 proxies that formed in connection with former positions of the
 sea. Once a sea-level indicator is measured and dated, it is
 necessary to establish its indicative meaning [89, 81] to quantify
 the relationship between the elevation or depth of an indicator
 and the position of the former sea level, including associated
 uncertainties due to the environmental range of formation. The
 corrected elevation of a sea-level indicator reflects paleo relative
 sea level (RSL), i.e., the paleo position of the sea including both
 barystatic (i.e., eustatic, 35) changes, elevation changes due to
 vertical land motions of different origin, and perturbations in the
 sea surface height.

On the GBR, corals of LIG age are presently preserved under a
 subsurface unconformity, which occurs down to 20-25 meters
 below present sea level, depending on the site [63, 40, 55, 78].

59
60
61
62
63
64
65
66
67
68
69
70
71
72
73
74
75

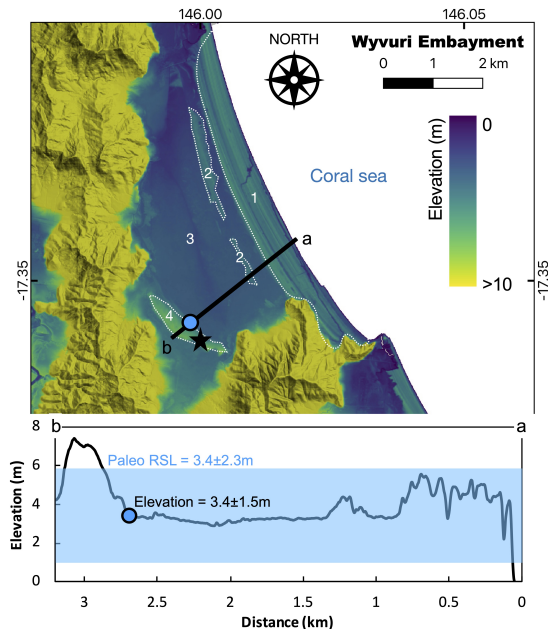


Figure 2: Digital Elevation Model [31] and topographic profile (a-b) of the Wyvuri Embayment, where Gagan et al. [30] identified LIG coastal sediments in a core under a dune/beach barrier. The star indicates the approximate point where core JW4 of Gagan et al. [30] was drilled. Numbers 1-4 indicate the facies reported in Gagan et al. [30]: 1-Holocene beach barrier; 2 - Holocene back-barrier; 3 - Holocene freshwater swamp; 4 - Last Interglacial beach barrier. The blue dot indicates the inner part of the LIG barrier used as a sea-level proxy in this study. The blue transparent overlay on the topographic profile indicates the paleo RSL calculated using the elevation of the inner margin of the barrier and the indicative meaning calculator tool [54].

coral island. This dated reef was not included among those reported in this work as we could not find enough information to produce a reliable sea-level index point from the information provided in Ryan et al. [78].

Murray-Wallace and Belperio [63] report the presence of scattered coastal deposits of LIG age along the continental coasts of New South Wales and Southern Queensland. These were interpreted, according to their sedimentary and geomorphological characteristics, as beach barriers, estuarine deposits or dune-island barriers. These features are ubiquitous along the SE Queensland Fraser Island Coast and far north New South Wales coasts [33], where the LIG age of the deposits is confirmed by U-series on corals embedded in the sedimentary units or Amino Acid Racemization dates [63]. The LIG strandplains are often overlain by Holocene transgressive sequences. Similar deposits as those described in New South Wales and Southern Queensland are also present in our study area. However, in contrast to LIG reef sequences in the GBR, most of these strandplains are rarely assigned an age with absolute dating techniques. Their MIS 5e age has been inferred via analogy with the strandplains in New South Wales and Northern Queensland, chronostratigraphic correlation with lower younger (Holocene) units, and infinite radiocarbon ages. An expanding Optically Stimulated Luminescence chronology for these deposits is in progress [33], and shows that complete LIG strandplains are located inboard of the modern Holocene equivalents.

In far north Queensland, Gagan et al. [30] describes a LIG dune/beach barrier located onshore with respect to the Holocene equivalent at Wyvuri Embayment (Figure 2). According to Gagan et al. [30], the top of the barrier, composed of aeolian sediments, is located at +6m above modern sea-level (in our topographic profile in Figure 2 this plots slightly higher, 7.5m), while the beach barrier sands were intercepted about 4m below the surface, in drill cores. This elevation roughly corresponds to a break in slope on the coastal plain (3.4 ± 1.5 m), which can be interpreted as a shoreline angle. Considering this analog to a beach deposit, and using the formulas and values suggested by Lorscheid and Rovere [54] to calculate the indicative meaning in absence of modern analog data, we calculate that this strandplain indicates a LIG paleo RSL of 3.4 ± 2.7 m (Figure 2). At the nearby Cowley Beach strandplain, Brooke et al. [10] established that the strandplain beach ridge morphology tracked Holocene sea-level trends.

The surface expression of the Wyvuri Embayment LIG beach barrier can be found at other locations along the Queensland coast, with the shoreline angle located roughly at the same elevation as Wyvuri Embayment (yellow markers in Figure 1). Towards the south of our study area, near the border between Queensland and New South Wales, fossil corals embedded into beach/intertidal/shallow subtidal deposits at North Stradbroke Island, are overlain by Holocene transgressive deposits and were dated to MIS 5e [68, 69]. The original authors suggest that these would indicate a paleo sea level between 1 to 3m, which is consistent with the paleo sea level calculated from the other beach barriers described above.

Starting from the description of Gagan et al. [30] and high-resolution (5m) Digital Elevation Models from [31], we identified other locations scattered along the Queensland coast where the LIG has left a morphological imprint as an evident beach

76 Murray-Wallace and Belperio [63] highlight that while low-lying islands are scattered throughout the GBR, outcrops of
 77 Pleistocene reefs above modern sea level are absent. The only
 78 exception may be an exposed reef of apparently Pleistocene age
 79 at 1-4m above present sea level [40] at Digby Island [49, 50].
 80 However, the age of this reef has never been confirmed with
 81 absolute dating, and it will not be discussed further. Retrieval
 82 of LIG reef sections on the GBR has been historically done by
 83 coring through the Holocene reef down to the Holocene/LIG un-
 84 conformity. A full account of the best-preserved and best-dated
 85 Last Interglacial corals on the GBR, alongside the paleo water
 86 depth of the coralgal assemblages and sedimentary facies asso-
 87 ciated with them, is provided by Dechnik et al. [18]. These data
 88 were recently compiled into the standardized WALIS (World
 89 Atlas of Last Interglacial Shorelines) database by Chutcharavan
 90 and Dutton [14] (blue markers in Figure 1). In general, these
 91 reefs have paleo water depths < 3m or < 6m, therefore they de-
 92 veloped in very shallow waters. The shallowest reef unit dated
 93 to MIS 5e (131 ± 1 ka, after open-system U-series corrections)
 94 was recently reported at Holbourne Island [78], at ca. 5m below
 95 the Lowest Astronomical Tide. It is worth noting that this island
 96 is much closer to the shoreline (20 km vs more than 50km) and
 97 is morphologically different to those reported by Dechnik et al.
 98 [18], as it is a continental high island rather than a low-lying
 99

159 barrier on the strandplain, from which sea-level index points can
160 be derived (see Supplementary Materials for detailed maps of
161 each area and a spreadsheet containing sea-level interpretations,
162 similar to those shown in Figure 2). The elevation of these barriers
163 is consistent with those identified in northern New South
164 Wales, which preserve a LIG sea-level trend from a highstand
165 at $+6 \pm 0.5\text{m}$ at 129 ka BP to $+4\text{m}$ by 116 ka BP [33]. The
166 SE Queensland and northern New South Wales studies revealed
167 that regional coastal fault reactivation has occurred during the
168 Late Quaternary that has influenced the accommodation space
169 for strandplain deposition. Overall the Late Quaternary onshore
170 strandplains extending from far North Queensland to far northern
171 New South Wales indicate that Late Pleistocene strandplains
172 are preserved in the $+3$ to $+6\text{m}$ elevation. This is in stark contrast
173 to the offshore submerged record, suggesting a LIG paleo
174 relative sea level below the modern one.

175 The fact that LIG reefs in the GBR are found below the typical
176 elevation of reefs of the same age on passive continental margins
177 was discussed by Marshall and Davies [55], who attributed it
178 to a combination of long-term subsidence of the continental
179 margin and erosion of the Pleistocene reef framework during
180 glacial times. Differential Holocene reef growth rates seem to
181 indicate that the Central GBR is subsiding with respect to the
182 Northern and Southern GBR. Dechnik et al. [19] suggest that
183 this subsidence may be related to the re-activation of NNW-SSE
184 extensional faults along the eastern Queensland margin [79, and
185 references therein].

186 2 RESULTS & DISCUSSION

187 2.1 Reef isostasy

188 Coral reefs are created by the fixation of calcium carbonate
189 mostly by hermatypic corals and calcareous algae [96]. Reefs
190 respond to variations in sea-level by catching up, keeping up
191 or giving up. From the geophysical perspective, this results in
192 the creation of a mass of reef framework, which can exert a
193 significant load on the underlying crust. This loading causes an
194 isostatic response that is non-negligible. Hereafter, we define
195 the isostatic adjustment induced by coral reef building as “*reef*
196 *isostasy*”.

197 An illustration of how reef isostasy impacts the elevation of
198 a LIG reef measured today is shown in Figure 3. During the
199 LIG, a reef builds on top of an older reef surface (or the base-
200 ment, Figure 3A). This loading induces isostatic adjustment,
201 causing subsidence, or equivalently a relative sea-level rise. The
202 sea-level change ΔRSL magnitude induced by reef isostasy de-
203 pends on reef thickness as well as its geographic extent. Areas
204 with loads of smaller spatial scale are compensated more by
205 elastic stresses, resulting in a smaller magnitude relative sea
206 level change associated with reef isostasy. During a subsequent
207 glacial period of lower sea level, erosion and karstification may
208 lead to unloading-induced uplift that partially compensates for
209 the subsidence during reef-building (Figure 3B). However, we
210 do not model this process in this work, as the total mass change
211 since the Last Interglacial is dominated by reef growth, rather
212 than reef erosion.

213 An increase in local relative sea-level from crustal subsidence
214 induced by reef isostasy results in lower elevation LIG coral
215 sea-level markers today, (assuming no GMSL difference) com-

pared to their original elevation at the LIG. Therefore LIG coral
reef sea-level marker elevations must be corrected upwards to
account for reef isostasy, potentially resulting in higher recon-
structed LIG GMSL than prior estimates.

220 2.2 Modelling reef isostasy: fine vs. coarse resolution

221 The predicted magnitude of relative sea level change is sensitive
222 to the spatial scale of the load, in addition to the load thickness.
223 We first perform calculations using a 3D sea-level model, and
224 the “fine resolution grid” coral reef loading scenario with a
225 regional spatial resolution of 1 km that accounts for the fractional
226 area of reef coverage in each grid cell (Methods). We next
227 compute reef isostasy using the “coarse resolution grid” to assess
228 whether the lower resolution input accurately captures the crustal
229 deformation (and thus relative sea level) response to reef loading.
230 Note that these coarse resolution runs use a 1D GIA model set
231 up and a loading scenario that does not account for reef coverage
232 area resulting in a larger volume and mass load for the coarse
233 resolution case (Methods).

234 Figure 4 (right panels) shows the elevation change that a LIG
235 sea-level indicator would undergo from 122 to 0ka due to reef
236 isostasy (negative values signify that sea-level indicators experi-
237 enced subsidence since the LIG). Our fine resolution simulation
238 of reef isostasy in the Great Barrier Reef predicts a maximum
239 relative sea level change of 0.34m since the Last Interglacial
240 (Figure 4B). These maximum values are reached in Northeast-
241 ern Queensland and along the coastline of the southern GBR.
242 Our predictions for relative sea level change due to reef isostasy
243 suggest this process is small compared to other uncertainties on
244 the paleoelevation of LIG coral reefs (for example coral growth
245 depths, tides etc.). In contrast, the coarse resolution reef isostasy
246 calculations predict a maximum relative sea level change of
247 1.45 m since the Last Interglacial (Figure 4D). The discrepancy
248 between fine vs. coarse resolution models is due to the fact
249 that the fine resolution calculation involves a more localized
250 loading geometry (and thus reduced crustal deflection) due to
251 elastic compensation within the lithosphere, compared with the
252 coarse resolution case that overestimates the mass load by not
253 accounting for aerial extent on a finer resolution grid.

254 Because fine resolution modeling using the 3D sea-level model
255 is computationally expensive, we also tested whether a 1D sea-
256 level model could accurately capture the pattern and magnitude
257 of relative sea level change due to reef isostasy. We first used
258 the fine resolution coral reef loading scenario and multiplied
259 the loading grid by the fractional area of reef coverage on a
260 1 km scale. We then interpolated this loading scenario onto a
261 grid with $\sim 34\text{km}$ resolution to create a coarse grid that accounts
262 for fractional area of reef coverage (Figure 4E). We ran a 1D
263 sea-level model with this loading scenario using the same Earth
264 model as in the other 1D calculation. This simulation resulted in
265 a similar magnitude of reef isostasy as in the 3D fine resolution
266 model, with a maximum value of 0.4m of RSL change since the
267 LIG (Figure 4F). However, the spatial pattern does not reproduce
268 the signal along the southern Great Barrier Reef coastline shown
269 in the 3D fine resolution simulations. This difference is likely
270 due to the higher resolution associated with the 3D sea-level
271 simulation rather than 3D earth structure, as the coarse resolution
272 1D calculation does not capture the reef loading regions along
273 the central and southern Great Barrier Reef coastline.

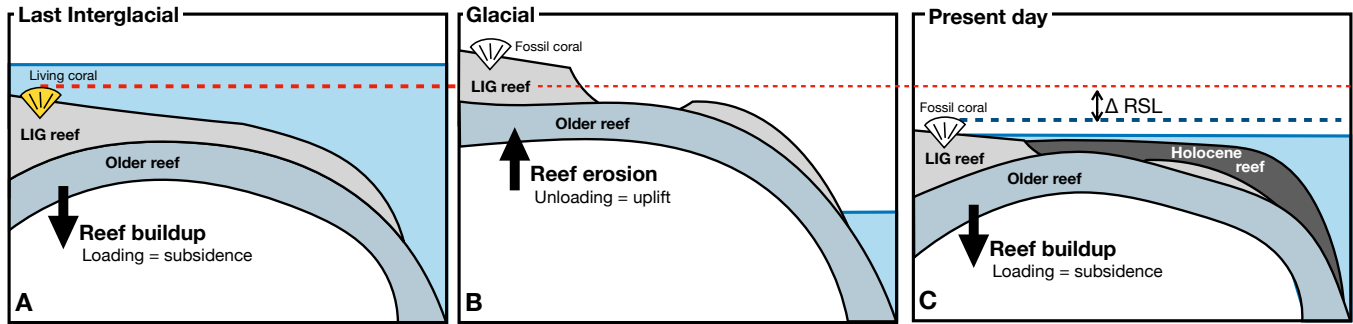


Figure 3: Illustration of reef isostasy caused by the buildup of the reef complex since the Last Interglacial. **A.** The LIG reef is built on top of an older reef (or the bedrock). The addition of this load leads to isostatic subsidence of the underlying bedrock. **B.** As GMSL falls (e.g., under glacial conditions), the reef is partially eroded and/or dissolved (e.g., by karst processes), resulting in isostatic rebound. **C.** As sea level rises a second time, the reef starts to build again on top of previous structures, causing additional subsidence. ΔRSL represents the relative sea-level change caused by reef isostasy. The colored dashed lines represent the elevation of the coral during the LIG (red) and its present-day elevation (blue). Note that the uplift and subsidence following reef loading and unloading are transient through glacial-interglacial times, and that in our study we do not model the uplift following reef erosion, which we consider to be balanced with Holocene re-growth.

274 To assess the sensitivity of our results to Earth structure parameters, we also performed 1D sea-level simulations using an alternate Earth model, VM2 [67]. We found that changing the Earth model had a negligible effect, perturbing the predicted RSL change by a maximum of 3% at the Queensland/GBR sea-level indicator sites.

280 2.3 Contribution of glacial isostatic adjustment and dynamic topography

282 We predicted the elevation change due to reef isostasy (Figure 5A), dynamic topography (Figure 5B), and glacial isostatic adjustment (Figure 5C) from 127ka to present (see Methods for details). These values represent the elevation change a LIG sea-level indicator would undergo from 127 to 0ka (negative values signify that sea-level indicators experienced subsidence, positive values signify that sea-level indicators experienced uplift since the LIG). The total predicted influence on Last Interglacial sea-level indicator elevation from these geodynamic processes is shown in Figure 5D.

292 Our dynamic topography predictions show an elevation change of -10 to 10m from 127 ka to present day, a rate of differential vertical motion that exceeds some regional estimates [20], but is comparable to others [41]. This means that dynamic topography would have uplifted the Australian continent by up to 10m, while offshore regions on the continental shelf would have subsided up to 5 to 10 m since the LIG. Variations in input density and viscosity structure lead to $\sim \pm 1$ m uncertainty in post-LIG dynamic topography change (based on standard deviation of 15 model predictions), and the spatial pattern is remarkably consistent amongst the 15 models investigated here. These results suggest that our predictions of convectively driven onshore-offshore tilting are robust. This inference is corroborated by ~ 100 m Myr^{-1} uplift rates inferred from river profile modelling [16] and patterns of Late Cenozoic age-independent magmatism [7], both features that have been attributed to the presence of an active small-scale convection cell beneath the Queensland margin. Although the dynamic topography maxima

and minima are offset with respect to the observed relative sea level maxima and minima, the highest horizontal resolution for the dynamic topography predictions is ~ 200 km, and therefore it may not be possible to precisely match the observed tilting at this resolution.

Similarly, glacial isostatic adjustment would have produced uplift on the continent and subsidence offshore. Our predictions show that the continent may have uplifted 6m and offshore regions subsided 2m since the Last Interglacial. The spatial variability in elevation change due to glacial isostatic adjustment is caused by the process known as continental levering, where uplift occurs along continental margins as sea-level rise causes subsidence in ocean basins due to water loading [60, 64].

In this study, we did not model several other potential mechanisms that may cause departure from eustasy in the study area. For example, crustal deformation due to re-activation of older faults has been inferred to affect Holocene reefs [see 79, and references therein]. While such a mechanism might have a relevant local effect, any fault system causing crustal motions would have to be active (with roughly the same deformation rates) over nearly 2000 km of coast to reconcile the observed onshore-offshore tilting trend. This seems an unlikely pattern in an intraplate margin setting such as the Queensland-GBR area. Another process we did not model is erosion and sediment deposition which drive a tilting (up on land) of the crust. Studies on the Central GBR shelf suggested that the thickness of Holocene sediments is rather limited [<2.5 m 46] hence siliciclastic sediment isostasy seems an unlikely explanation for the large difference between onshore and offshore LIG sea-level proxies, recorded over such a large latitudinal gradient.

An important caveat to our reef isostasy modeling is that we did not account for additional loading associated with other processes, such as carbonate sands (also mixed with siliciclastic sediments) close to modern reef areas [37], post-LGM reef buildups (now drowned on the shelf [37]), and other bioherms of considerable importance, such as inter-reefal *Halimeda* algal

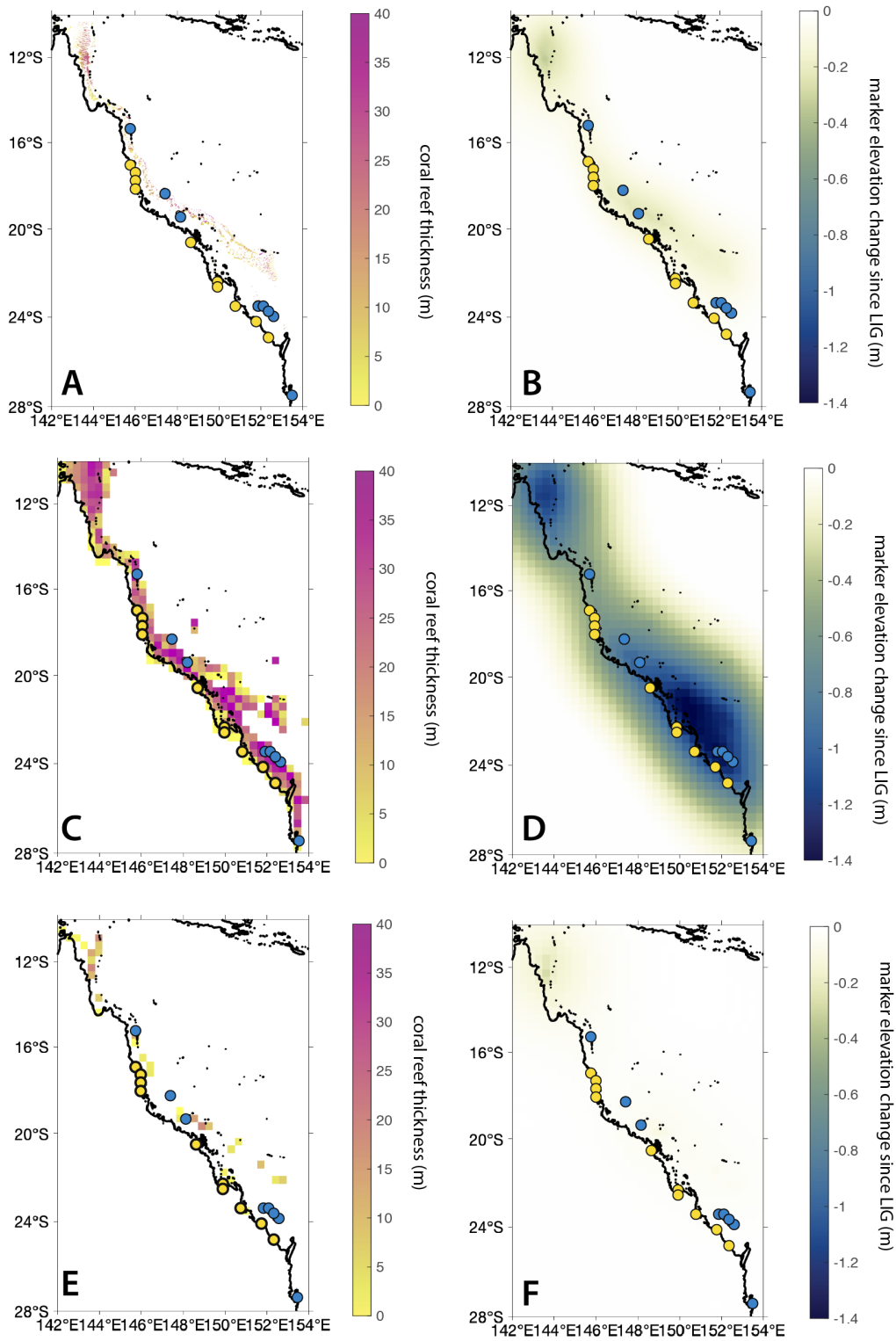


Figure 4: **A.** Fine resolution coral reef thickness (122-0ka) for the reef isostasy loading scenario. **B.** Predicted marker elevation change since LIG due to reef isostasy in response to loading in frame A. **C-D.** As in A-B, except for the coarse resolution modeling. **E-F.** As in C-D, except for the coarse resolution treatment of reef thickness (122-0ka) accounting for reef area coverage. Yellow and blue dots in each map represent the sites shown in Figure 1

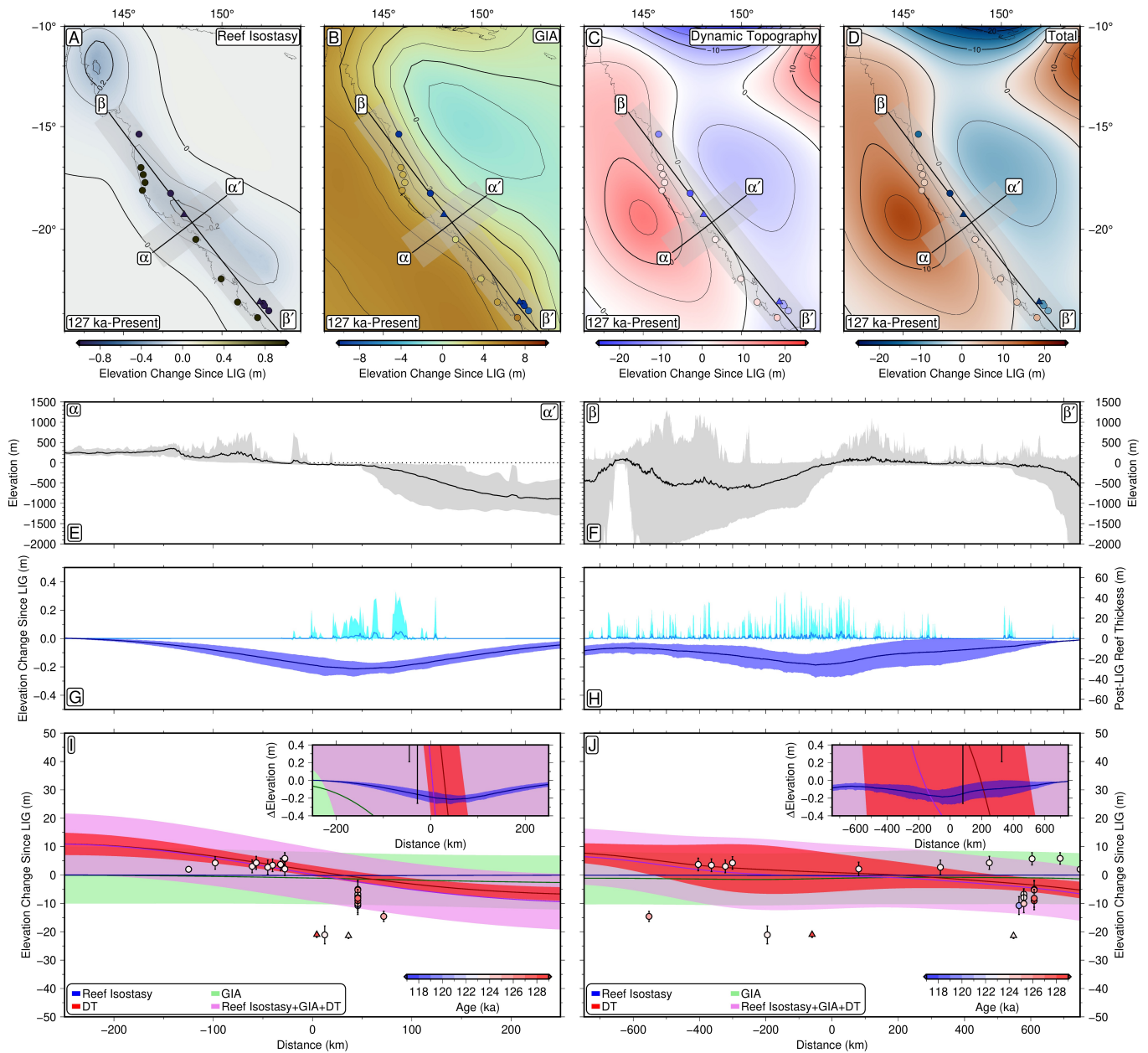


Figure 5: A-C. Predicted elevation change to sea-level indicators from 127 to 0ka due to: A. reef isostasy B. glacial isostatic adjustment C. dynamic topography. Colored circles represent LIG sea-level indicators as shown in Figure 1. D. Total predicted elevation change to sea-level indicators from 127 to 0ka. E-F. Gray represents observed elevation range and black line represents mean values for transect α - α' (left) and β - β' (right). G-H. Light blue line and envelope represents the observed range in reef thicknesses in coral reef loading scenario from LIG to present. Dark blue line and envelope represents the predicted elevation change to sea-level markers due to reef isostasy (as in Figure 5A). Lines represent mean values based on spatial uncertainty of 100km on either side of transect and intermodel variation uncertainty; envelopes represent the 2 sigma combined uncertainty. I-J. GBR LIG sea-level data points projected onto transects α - α' (left) and β - β' as a function of distance between the data point and the closest point on the transect. Colored circles/triangles represent LIG sea-level indicator ages. Predicted elevation change projected onto transect A (left) and B (right) for reef isostasy (blue), dynamic topography (red), glacial isostatic adjustment (green), and total (pink). Lines and envelope calculated as in G-H

346 buildups [57]. Including these factors would increase the load
 347 and hence the relative importance of reef isostasy, however it
 348 is unlikely to explain the large differences between the onshore
 349 and offshore LIG sea-level indicators.

350 3 CONCLUSIONS

351 The Queensland - GBR area is characterized by an enigmatic
 352 difference in the elevation of LIG sea-level indicators between
 353 offshore (GBR) and onshore (Queensland coast) sites. This
 354 offset motivated our modeling of local post-depositional vertical
 355 land motion. We modelled sea-level change due to reef isostasy,
 356 dynamic topography, and glacial isostatic adjustment since the
 357 LIG in this area, which is located on a passive margin spanning
 358 a latitudinal range of almost 2000 km. Our models explored
 359 whether reef isostasy, which is considered here for the first
 360 time, may play a role in the observed vertical displacement of
 361 LIG fossil reefs, which are among the most frequently used
 362 geological sea-level proxies [87, 21, 65].

363 Our results show that the contribution of reef isostasy to vertical
 364 land motions is negligible, reaching maximum values of 0.34m.
 365 In comparison with GMSL changes, this is roughly equivalent to
 366 half the contribution to GMSL of mountain glaciers melting and
 367 thermal expansion during the LIG (estimated as up to 1m; 22).
 368 Reef isostasy therefore produces a relatively small change in
 369 RSL since the LIG at the GBR, and is insufficient in magnitude
 370 to explain discrepancies between observed LIG RSL markers
 371 offshore and onshore. However, we emphasize that the load we
 372 constructed might be an underestimation, so this mechanism
 373 may represent a potentially important contribution to vertical
 374 land motions in areas with dense and widespread coral reef
 375 coverage. Therefore, neglecting reef isostasy may represent a
 376 potential bias in areas with widespread reef coverage.

377 To realistically represent coral reef loading since the LIG in a
 378 given area, it is important to gather direct measurements of reef
 379 thickness, extent, density and porosity, together with estimates
 380 of mass loss since the LIG (e.g., due to erosion or karst pro-
 381 cesses, which we do not model here) and, in the case of wide
 382 lagoons, carbonate sediment production rates from the reef. In
 383 addition, the presence of other buildups other than coral reefs,
 384 capable of producing relevant loads at wide spatial scales, are
 385 important. Our results underscore the importance of fine resolu-
 386 tion modeling, especially in accounting for the areal coverage
 387 of coral reefs, to accurately reproduce relative sea level change
 388 due to reef isostasy. Once these data are available, we show that
 389 while 1D sea-level models are more computationally efficient,
 390 for small-scale loading patterns such as coral reefs, it may be im-
 391 portant to use high resolution 3D modeling to accurately capture
 392 the relative sea level response to reef loading.

393 Comparing the modeled relative contributions of reef isostasy,
 394 dynamic topography, and glacial isostatic adjustment, we sur-
 395 mise that only the predicted change due to dynamic topography
 396 across sites has a magnitude similar to the differences in sea-
 397 level indicator elevations between onshore and offshore. This
 398 result strengthens the argument that dynamic topography may
 399 play a major role in the vertical displacement of LIG sea-level
 400 indicators at Late Pleistocene time scales [5], and cannot be
 401 ignored, even at passive margins, in MIS 5e sea-level reconstruc-
 402 tions.

4 METHODS

4.1 Constructing the coral reef loading scenario

405 As a baseline dataset for the presence/absence of coral reefs, we
 406 used the 500 × 500m raster dataset [12, 13, 44] of the warm-
 407 water reefs map compiled by UNEP-WCMC, WorldFish Centre,
 408 WRI, TNC [88, 42, 43, 83]. We created a coral reef loading
 409 scenario since the LIG (122-0 ka) using two methods, with
 410 different resolutions. For the "coarse resolution grid", we used a
 411 standard approach for sea-level model calculations and placed
 412 our coral loading scenario onto a ~34 km resolution grid. For
 413 the "fine resolution grid", we placed our coral loading scenario
 414 onto a 1 km resolution grid, and accounted for the areal fraction
 415 of coral reef coverage within each 1 km x 1 km grid cell.

416 Because the GBR reef is characterized by narrow, sometimes
 417 isolated, strips of coral reef, we were concerned that the stan-
 418 dard grid resolution (~34 km) used in sea-level models may
 419 unrealistically smooth out the reef loading signal. Thus, for the
 420 "fine resolution grid" we interpolated a high-resolution Digital
 421 Elevation Model for bathymetry in the Great Barrier Reef area
 422 onto a 1 km resolution grid [9]. We then assessed the fractional
 423 area of reef coverage within each 1 km × 1 km grid cell using
 424 the "Fishnet" tool of ArcGIS. Of grid cells with non-zero reef
 425 coverage, 44% had full reef coverage (Figure 6). We then multi-
 426 plied the coral reef thickness in our 1 km x 1 km grids by the
 427 areal fraction of reef coverage to produce our "fine resolution
 428 grid" coral reef loading scenario.

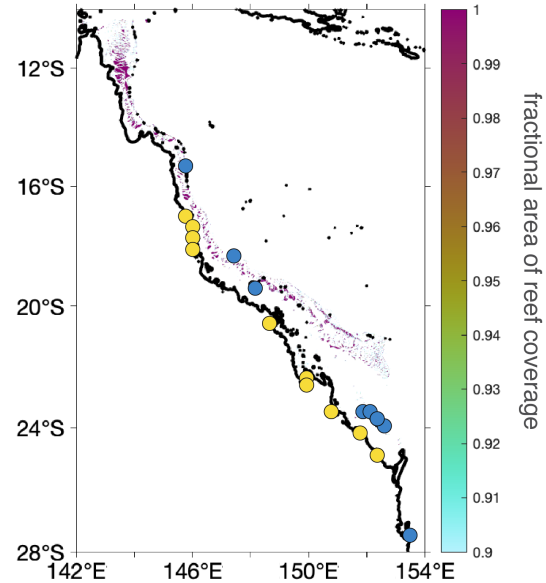


Figure 6: Fractional area of present-day reef coverage. Yellow and blue dots represent the sites shown in Figure 1.

429 We also used a standard approach for constructing a loading
 430 scenario by interpolating a high-resolution bathymetric Digital
 431 Elevation Model of the GBR area onto a Gauss Legendre grid
 432 with ~34 km resolution (maximum spherical harmonic degree
 433 512) commonly used in sea-level calculations. This approach
 434 does not account for coral reef coverage since the coral reef
 435 thickness is smoothed over a wide area relative to the lateral

436 extent of coral reefs. We term this coral reef loading scenario
437 the “coarse resolution grid” (Figure 4C).

438 Apart from a very small number of examples, including the
439 Ribbon Reef Core in the Northern GBR outer shelf (155 m
440 reefal thickness), Boulder Reef core northern GBR mid shelf
441 (33 m reefal thickness) [93], and One Tree Reef core Southern
442 GBR mid shelf (18 m reefal thickness) [19], the total vertical
443 extent of reef buildups since the LIG is largely unknown.
444 Limited seismic stratigraphy of the GBR has focused on the
445 inter-reefal shelf areas and show the shelf comprising Permo-
446 Carboniferous bedrock, Pleistocene/Tertiary sediments, consist-
447 ing of both shelf-wide terrigenous units, and carbonate mounds
448 and platforms under present reefs [46]. Given these limited
449 datasets, the thickness of individual reefs was calculated using
450 the average shelf depth surrounding reef structures, with positive
451 relief above this surface representing reef aggradation across the
452 Pleistocene/Holocene.

453 Following the above, in both scenarios, we assumed that regions
454 with any reef coverage (fractional area of reef coverage > 0 ;
455 Figure 6A) had coral reefs that had grown since the LIG. We
456 assigned the total coral reef thickness deposited since the LIG as
457 the modern basement depth (i.e., we assumed the coral reef sur-
458 face grew to modern sea level) in regions with basement depths
459 shallower than 55 m. Below this bathymetry, we considered
460 that no reef was present during the LIG. To partition coral reef
461 loading across 122 to 0 ka, we made the assumption that the
462 Last Interglacial reef thickness would represent 1.5 times the
463 thickness of Holocene coral reef growth, given the longer time
464 available for LIG reefs to grow with respect to Holocene ones.
465 In our models, we assumed a reef porosity of 40% (that is, the
466 porosity of reefs in sand flats/lagoons in the GBR reported by
467 39) and a coral reef density of 1600 kg/m³ (equivalent to the
468 average coral colony density as reported by 11 in 39).

469 For the “fine resolution grid” coral loading scenario, we mul-
470 tiplied our map of reef thickness by the fractional area of reef
471 coverage (Figure 6A). This assumes that the coverage hasn’t
472 changed since 120 ka. Accounting for the aerial extent on a fine
473 resolution grid results in a reduced mass load compared to the
474 “coarse resolution grid” that does not account for fractional area
475 of reef coverage. The fine resolution grid is characterized by a
476 total volume of 3.1×10^{11} m³ (Figure 4A), whereas the coarse
477 resolution grid’s load is greater by an order of magnitude, with
478 a total volume of 5.6×10^{12} m³ (Figure 4C). The last reef loading
479 scenario that accounts for aerial extent by interpolating the fine
480 resolution loading scenario onto the coarser grid (Figure 4E)
481 results in a substantially smaller total volume (2.2×10^8 m³), de-
482 spite predicting a similar magnitude of relative sea level change
483 compared with that associated with the fine resolution simulation
484 (Figure 4B and F).

485 To isolate the impact of reef loading, we did not include ice sheet
486 loading changes in our modeling. Our reef loading scenario
487 introduced the LIG coral thickness at 120 ka and the Holocene
488 coral thickness at 8 ka. Although coral reefs are built over a
489 longer time span, we simplified our calculation by introducing
490 the load at a single timestep, assuming that the timing of the
491 load will have a negligible impact at present-day after several
492 thousand years of isostatic adjustment. To conserve mass, we
493 uniformly removed a layer of sediment from the continents with
494 a mass equivalent to the total reef load globally.

495 Although reef loading prior to the LIG would have induced an
496 ongoing isostatic response at the LIG, our analysis is limited to
497 estimating sea-level change since the LIG due to reef loading
498 over only the last glacial cycle. Thus, we limited our modeling
499 to the period from 122 to 0 ka to assess the magnitude of sea
500 level change due to reef loading since 122 ka.

4.2 Modeling Isostatic Adjustment: Reef isostasy

501 **1D calculation (coarse resolution).** To calculate relative sea-
502 level change (Δ RSL) in response to reef loading over the last ice
503 age, we used a gravitationally self-consistent sea-level model.
504 We used the coarse resolution coral reef loading scenario as in-
505 put to a 1D sea-level model, which assumes radially symmetric
506 Earth structure. Our calculations are based on the theory and
507 pseudo-spectral algorithm described by Kendall et al. [48] with
508 a spherical harmonic truncation at degree and order 512 (spatial
509 resolution of ~ 34 km). These calculations include the impact of
510 load-induced Earth rotation changes on sea level [58, 62], evol-
511 ving shorelines and the migration of grounded, marine-based ice
512 [47, 59, 52, 48]. Our predictions require models for Earth’s vis-
513 coelastic structure. We adopted an earth model characterized by
514 a lithospheric thickness of 96 km, and upper and lower mantle
515 viscosities of 5×10^{20} and 5×10^{21} Pa s, respectively.
516

517 **3D calculation (fine resolution).** To solve for relative sea level
518 change in response to coral reef loading on a higher resolution
519 of 1 km, we used a global 3D finite volume sea level and Earth
520 deformation model [53]. The numerical approach incorporates
521 lateral variations in Earth structure and calculates the resulting
522 gravitationally self-consistent sea level change [61]. Previous
523 studies have adopted this computational model in order to ac-
524 count for 3D earth structure (e.g., 4, 32, 51). The 3D glacial
525 isostatic adjustment model is capable of km-scale resolution,
526 which is achieved through regional grid refinement for compu-
527 tational efficiency [32]. The importance of fine resolution GIA
528 modeling has been demonstrated for the solid Earth response
529 to marine grounding line migration in Antarctica [92]. Grid
530 refinement is achieved by incrementally bisecting grid edges in
531 the selected region to achieve the desired 1 km x 1 km resolution,
532 and a final smoothing operation along the region boundary to
533 ensure a well-behaved transition.

534 Our simulation uses a 3D viscoelastic earth model. Here, we
535 apply the hybrid model described in Austermann et al. [6], which
536 infers mantle viscosity from seismic tomography using anelastic
537 scaling relationships and additional information on the thermal
538 and rheological state of the upper mantle. In the upper 400 km,
539 a calibrated parameterisation of anelastic behaviour at seismic
540 frequencies is used to self-consistently determine lithospheric
541 thickness (assumed here to be equivalent to 1175°C isotherm
542 depth) and viscosity variations from the shear-wave velocity (V_S)
543 structure of the tomographic model, SL2013sv [72, 80]. Below
544 400km, viscosities are derived from the shear wave tomography
545 model SEMUCB-WM1 [29]. Austermann et al. (2021) [6]
546 provides details on the V_S to viscosity conversion.

547 In our 3D GIA calculations, viscosity variations are shifted at
548 each depth to average to 5×10^{20} Pa s in the upper mantle vis-
549 cosity 5×10^{21} Pa s in the lower mantle viscosity [71], identical
550 to the earth model used in the 1D GIA calculations. The ef-
551 fective lithospheric thickness in this region varies from 50–100
552 km (Figure S1). We paired this model with the fine resolution

553 coral reef loading scenario (Figure 4A) which accounts for reef
554 coverage area at 1 km resolution (Figure 6).

555 4.3 Modeling Glacial Isostatic Adjustment: Ice loading

556 We modeled relative sea level change in response to ice sheet
557 and ocean loading changes since the LIG using the 1D pseudo-
558 spectral approach described in Kendall et al. [48]. We used the
559 same model and earth structure described in the 1D reef loading
560 sea-level calculations.

561 We used an ice history characterized by the GMSL history in
562 Waelbroeck et al. [90] over the last glacial cycle. The ice history
563 was constructed using the ICE-6G deglacial ice geometry history
564 and has no excess melt across the LIG (as in 6). The GMSL
565 history was adjusted at the LIG since the Waelbroeck GMSL
566 history assumes a value of -75 m at 128 ka, which is at odds with
567 coral evidence from the many locations that indicate sea level
568 must have been close to present at that time. To account for this
569 discrepancy, the timing of the GMSL curve is shifted back prior
570 to the LIG by 3.5 ka. This shift allows for a longer interglacial
571 time period without changing the deglaciation pattern of the
572 original curve and places the MIS 6 sea-level low stand at 135.5
573 ka (as in 24).

574 4.4 Dynamic Topography

575 Observational estimates indicate that mantle flow-driven ver-
576 tical motions can reach rates of ~ 0.1 - 1 m kyr⁻¹ in certain lo-
577 cations, suggesting a significant fraction of relative sea-level
578 change along the Great Barrier Reef from the LIG to present
579 day could result from evolving mantle dynamic topography
580 [36, 91, 5, 85]. To investigate this possibility, we simulate rates
581 of global dynamic topography change using the mantle convec-
582 tion code ASPECT and an ensemble of Earth models based on
583 5 seismic tomographic inversions of deep Earth structure (LLNL-
584 G3D-JPS, 82; S40RTS, 74; SAVANI, 3; SEMUCB-WM1, 29;
585 TX2011, 34) and 3 radial viscosity profiles (S10, 84; F10V1,
586 28; F10V2, 28).

587 Above 300 km, input temperature and density fields are de-
588 termined from seismic velocity using an experimentally de-
589 rived parameterisation of rock anelasticity at seismic frequencies
590 [97]. Uncertain parameters in this formulation are calibrated
591 using a range of independent observational constraints on the
592 co-variation of upper mantle V_S , temperature, attenuation, and
593 viscosity (see 72 for details). This approach ensures that the
594 mapping between seismic velocities and buoyancy variations is
595 thermomechanically self-consistent, while also partially correct-
596 ing for discrepancies between tomographic models that result
597 from parameterisation choices rather than true Earth structure.
598 Here, the seismic velocity model we use to obtain upper mantle
599 structure is SLNAAFSA, a version of the SL2013sv upper man-
600 tle model [80] into which a number of high-resolution regional
601 updates have been incorporated (see 38 for details). This input
602 structure is chosen since it produces geodynamic predictions that
603 are in good agreement with landscape evolution [86], mantle
604 potential temperature [8], and residual depth observations, even
605 at relatively short wavelengths (~ 1000 km; 72).

606 Below 400 km, a thermodynamic modelling approach is used
607 to obtain thermochemical buoyancy structures for each combi-
608 nation of seismic tomographic and rheological input that are

compatible with present-day geophysical observables, includ-
ing geoid anomalies, dynamic topography, and CMB excess
ellipticity, and comprise thermochemical anomalies within the
base of LLVPs (73; see Supplementary Material for further
details). Note that, although LLVPs have limited impact on
LIG-to-present dynamic topography change, our calculations of
the RSL change induced by mantle flow account for associated
geoid variations (see Supplementary Material for further details).
Since these gravitational changes are more sensitive to the deep
mantle, incorporation of accurate LLVP structure in our global
convection simulation produces a non-negligible improvement
in the reliability of our predictions. Between 300 and 400 km,
temperatures and densities derived from these two independent
parameterisations are smoothly merged by taking their weighted
average as a function of depth.

The time-dependent geodynamic simulations derived from these
Earth models assume free-slip conditions at the surface and core-
mantle boundary, account for lithospheric cooling by including
shallow mantle buoyancy variations and representative thermal
conductivity, and incorporate temperature- and composition-
dependent viscosity variations (see Supplementary Material for
further details). Following [5], we run our models forward in
time and, to avoid the potential for transient numerical artefacts
in early time steps to affect our results, we assume the average
rate of dynamic topography change between 0.5 and 1.5 Ma
is representative of that experienced between the LIG and the
present day. Change in dynamic topography at specific sea-
level sites is calculated by combining perturbations due to the
evolving mantle flow pattern with those caused by rigid plate
motion across the convective planform. This is accomplished by
translating the dynamic topography field calculated for the LIG
into its present-day coordinates using plate velocities taken from
MORVEL [2], before calculating the difference between this
rotated LIG field and the predicted present-day field, yielding a
total of 15 individual model predictions (5 tomography models
combined with 3 viscosity profiles). Note that the maximum
horizontal resolution of the tomographically derived Earth mod-
els is ~ 200 km, placing an important limit on the minimum
wavelength of predicted dynamic topography variations.

575 5 DATA AVAILABILITY

Supplementary figures and the datasets used in this study are
available open-access as Rovere et al. [76].

585 6 AUTHOR CONTRIBUTIONS

The manuscript was written jointly by A.R. and T.P. The initial
concept of this work was developed by A.R., M.J.O., I.D.G. and
J.X.M. Models of reef isostasy were developed by T.P. Models
of dynamic topography and glacial isostatic adjustment were
developed by F.R., J.A. and K.L. The parts of the manuscript
related to field observations was written by A.R., M.J.O. and
I.D.G. The parts of the manuscript related to modelled vertical
land motions were written by T.P. and F.R. with inputs from
J.X.M., J.A. and K.L.

7 ACKNOWLEDGMENTS

This work was funded by the European Research Council (ERC) under the European Union’s Horizon 2020 research and innovation programme (grant agreement n. 802414 to A.R.). T.P. acknowledges funding from the NSF EAR Postdoctoral Fellowship, the University of California President’s Postdoctoral Fellowship, and NSF OCE – 2054757. F.D.R. acknowledges funding from the Imperial College Research Fellowship Scheme. J.A. acknowledges funding from NSF grant OCE-1841888. Funding is also acknowledged from Harvard University (J.X.M. and K.L.)

REFERENCES

- [1] P. N. Adams, N. D. Opdyke, and J. M. Jaeger. Isostatic uplift driven by karstification and sea-level oscillation: Modeling landscape evolution in north florida. *Geology*, 38(6): 531–534, 2010.
- [2] D. F. Argus, R. G. Gordon, and C. DeMets. Geologically current motion of 56 plates relative to the no-net-rotation reference frame. *Geochemistry, Geophysics, Geosystems*, 12(11), 2011.
- [3] L. Auer, L. Boschi, T. Becker, T. Nissen-Meyer, and D. Giardini. Savani: A variable resolution whole-mantle model of anisotropic shear velocity variations based on multiple data sets. *Journal of Geophysical Research: Solid Earth*, 119(4):3006–3034, 2014.
- [4] J. Austermann, J. X. Mitrovica, K. Latychev, and G. A. Milne. Barbados-based estimate of ice volume at last glacial maximum affected by subducted plate. *Nature Geoscience*, 6(7):553–557, 2013.
- [5] J. Austermann, J. X. Mitrovica, P. Huybers, and A. Rovere. Detection of a dynamic topography signal in last interglacial sea-level records. *Science Advances*, 3(7): e1700457, 2017.
- [6] J. Austermann, M. J. Hoggard, K. Latychev, F. D. Richards, and J. X. Mitrovica. The effect of lateral variations in earth structure on last interglacial sea level. *Geophysical Journal International*, 227(3):1938–1960, 2021.
- [7] P. Ball, K. Czarnota, N. White, M. Klöcking, and D. Davies. Thermal structure of eastern australia’s upper mantle and its relationship to cenozoic volcanic activity and dynamic topography. *Geochemistry, Geophysics, Geosystems*, 22(8):e2021GC009717, 2021.
- [8] P. Ball, N. White, J. Maclennan, and S. Stephenson. Global influence of mantle temperature and plate thickness on intraplate volcanism. *Nature communications*, 12(1):1–13, 2021.
- [9] R. Beaman. High-resolution depth model for the great barrier reef and coral sea - 100 m, 2020.
- [10] B. P. Brooke, Z. Huang, W. A. Nicholas, T. S. Oliver, T. Tamura, C. D. Woodroffe, and S. L. Nichol. Relative sea-level records preserved in holocene beach-ridge strandplains—an example from tropical northeastern australia. *Marine Geology*, 411:107–118, 2019.
- [11] R. W. Buddemeier, J. E. Maragos, and D. W. Knutson. Radiographic studies of reef coral exoskeletons: rates and patterns of coral growth. *Journal of Experimental Marine Biology and Ecology*, 14(2):179–199, 1974.
- [12] L. Burke, K. Reytar, M. Spalding, and A. Perry. Reefs at risk revisited: technical notes on modeling threats to the world’s coral reefs. *Washington, DC: World Resources Institute*, 2011.
- [13] L. Burke, K. Reytar, M. Spalding, and A. Perry. *Reefs at risk revisited*. World Resources Institute, 2011.
- [14] P. M. Chutcharavan and A. Dutton. A global compilation of u-series-dated fossil coral sea-level indicators for the last interglacial period (marine isotope stage 5e). *Earth System Science Data*, 13(7):3155–3178, 2021. doi: 10.5194/essd-13-3155-2021. URL <https://essd.copernicus.org/articles/13/3155/2021/>.
- [15] J. R. Creveling, J. Austermann, and A. Dutton. Uplift of trail ridge, florida, by karst dissolution, glacial isostatic adjustment, and dynamic topography. *Journal of Geophysical Research: Solid Earth*, 2019.
- [16] K. Czarnota, G. Roberts, N. White, and S. Fishwick. Spatial and temporal patterns of australian dynamic topography from river profile modeling. *Journal of Geophysical Research: Solid Earth*, 119(2):1384–1424, 2014.
- [17] A. Dalca, K. Ferrier, J. X. Mitrovica, J. Perron, G. Milne, and J. Creveling. On postglacial sea level—iii. incorporating sediment redistribution. *Geophysical Journal International*, 194(1):45–60, 2013.
- [18] B. Dechnik, J. M. Webster, G. E. Webb, L. Nothdurft, A. Dutton, J. C. Braga, J.-x. Zhao, S. Duce, and J. Sadler. The evolution of the great barrier reef during the last interglacial period. *Global and Planetary Change*, 149:53–71, 2017.
- [19] B. Dechnik, J. M. Webster, G. E. Webb, L. Nothdurft, and J.-x. Zhao. Successive phases of holocene reef flat development: Evidence from the mid- to outer great barrier reef. *Palaeogeography, Palaeoclimatology, Palaeoecology*, 466:221–230, 2017. ISSN 0031-0182. doi: <https://doi.org/10.1016/j.palaeo.2016.11.030>. URL <https://www.sciencedirect.com/science/article/pii/S0031018216304412>.
- [20] L. DiCaprio, M. Gurnis, R. D. Müller, and E. Tan. Mantle dynamics of continentwide cenozoic subsidence and tilting of australia. *Lithosphere*, 3(5):311–316, 2011.
- [21] A. Dutton and K. Lambeck. Ice volume and sea level during the last interglacial. *science*, 337(6091):216–219, 2012.
- [22] A. Dutton, A. E. Carlson, A. J. Long, G. A. Milne, P. U. Clark, R. DeConto, B. P. Horton, S. Rahmstorf, and M. E. Raymo. Sea-level rise due to polar ice-sheet mass loss during past warm periods. *science*, 349(6244):aaa4019, 2015.
- [23] A. Dutton, J. M. Webster, D. Zwartz, K. Lambeck, and B. Wohlfarth. Tropical tales of polar ice: evidence of last interglacial polar ice sheet retreat recorded by fossil reefs of the granitic seychelles islands. *Quaternary Science Reviews*, 107:182–196, 2015.
- [24] B. Dyer, J. Austermann, W. J. D’Andrea, R. C. Creel, M. R. Sandstrom, M. Cashman, A. Rovere, and M. E. Raymo.

- 773 Sea-level trends across the Bahamas constrain peak last
774 interglacial ice melt. *Proceedings of the National Academy
775 of Sciences of the United States of America*, 118(33):1–11,
776 2021. ISSN 10916490. doi: 10.1073/pnas.2026839118.
- 777 [25] W. Farrell and J. A. Clark. On postglacial sea level. *Geo-
778 physical Journal International*, 46(3):647–667, 1976.
- 779 [26] K. L. Ferrier, J. X. Mitrovica, L. Giosan, and P. D. Clift.
780 Sea-level responses to erosion and deposition of sediment
781 in the indus river basin and the arabian sea. *Earth and
782 Planetary Science Letters*, 416:12–20, 2015.
- 783 [27] K. L. Ferrier, J. Austermann, J. X. Mitrovica, and T. Pico.
784 Incorporating sediment compaction into a gravitationally
785 self-consistent model for ice age sea-level change. *Geo-
786 physical Journal International*, 211(1):663–672, 2017.
- 787 [28] A. M. Forte, S. Quéré, R. Moucha, N. A. Simmons, S. P.
788 Grand, J. X. Mitrovica, and D. B. Rowley. Joint seismic–
789 geodynamic–mineral physical modelling of African geody-
790 namics: A reconciliation of deep-mantle convection with
791 surface geophysical constraints. *Earth and Planetary Sci-
792 ence Letters*, 295(3–4):329–341, 2010.
- 793 [29] S. W. French and B. Romanowicz. Broad plumes rooted
794 at the base of the Earth’s mantle beneath major hotspots.
795 *Nature*, 525(7567):95–99, 2015. ISSN 0028-0836. doi:
796 10.1038/nature14876.
- 797 [30] M. K. Gagan, D. P. Johnson, and G. M. Crowley. Sea
798 level control of stacked late quaternary coastal sequences,
799 central great barrier reef. *Sedimentology*, 41(2):329–351,
800 1994.
- 801 [31] Geoscience Australia. *Digital Elevation Model (DEM)
802 of Australia derived from LiDAR 5 Metre Grid*. Aus-
803 tralian Government, Canberra, 2015. doi: [https://doi.org/
804 10.26186/89644](https://doi.org/10.26186/89644).
- 805 [32] N. Gomez, K. Latychev, and D. Pollard. A coupled ice
806 sheet–sea level model incorporating 3d earth structure:
807 Variations in antarctica during the last deglacial retreat.
808 *Journal of Climate*, 31(10):4041–4054, 2018.
- 809 [33] I. D. Goodwin. Last interglacial sea-level and wave climate
810 change in the subtropical south-west pacific. in prep.
- 811 [34] S. P. Grand. Mantle shear–wave tomography and the fate of
812 subducted slabs. *Philosophical Transactions of the Royal
813 Society of London. Series A: Mathematical, Physical and
814 Engineering Sciences*, 360(1800):2475–2491, 2002.
- 815 [35] J. M. Gregory, S. M. Griffies, C. W. Hughes, J. A. Lowe,
816 J. A. Church, I. Fukimori, N. Gomez, R. E. Kopp, F. Lan-
817 derer, G. L. Cozannet, R. Ponte, D. Stammer, M. E.
818 Tamisiea, and R. S. W. van de Wal. Concepts and ter-
819 minology for sea level: Mean, variability and change, both
820 local and global. *Surveys in Geophysics*, 40(6):1251–1289,
821 2019.
- 822 [36] R. A. Hartley, G. G. Roberts, N. White, and C. Richardson.
823 Transient convective uplift of an ancient buried landscape.
824 *Nature Geoscience*, 4(8):562–565, 2011.
- 825 [37] G. Hinestrosa, J. M. Webster, and R. J. Beaman. Post-
826 glacial sediment deposition along a mixed carbonate-
827 siliciclastic margin: New constraints from the drowned
shelf-edge reefs of the great barrier reef, australia. *Palaeo-
geography, Palaeoclimatology, Palaeoecology*, 446:168–
185, 2016.
- [38] M. J. Hoggard, K. Czarnota, F. D. Richards, D. L. Huston,
A. L. Jaques, and S. Ghelichkhan. Global distribution of
sediment-hosted metals controlled by craton edge stability.
Nature Geoscience, 13:504–510, 2020.
- [39] D. Hopley. *Density and Porosity Density and Porosity: In-
fluence on Reef Accretion Rates*, pages 303–304. Springer
Netherlands, Dordrecht, 2011. ISBN 978-90-481-2639-
2. doi: 10.1007/978-90-481-2639-2_275. URL https://doi.org/10.1007/978-90-481-2639-2_275.
- [40] D. Hopley, S. G. Smithers, and K. Parnell. *The geomor-
phology of the Great Barrier Reef: development, diversity
and change*. Cambridge University Press, 2007.
- [41] L. Husson, N. Riel, S. Aribowo, C. Authemayou,
G. de Gelder, B. Kaus, C. Mallard, D. Natawidjaja, K. Pe-
doja, and A. Sarr. Slow geodynamics and fast morphotec-
tonics in the far east tethys. *Geochemistry, Geophysics,
Geosystems*, 23(1):e2021GC010167, 2022.
- [42] IMaRS-USF. Millennium coral reef mapping project. un-
validated maps, 2005.
- [43] IMaRS-USF, IRD. Millennium coral reef mapping project.
validated maps, 2005.
- [44] Institute for Marine Remote Sensing, University of South
Florida (IMaRS/USF) Institut de Recherche pour le
Développement (IRD), UNEP-WCMC, The WorldFish
Center, and WRI,. Global Coral Reefs composite dataset
compiled from multiple sources for use in the Reefs at Risk
Revisited project incorporating products from the Millen-
nium Coral Reef Mapping Project prepared by IMaRS/USF
and IRD, 2011.
- [45] IPCC. *Ipc special report on the ocean and cryosphere in
a changing climate*. 2019.
- [46] D. Johnson and D. Searle. Post-glacial seismic stratigraphy,
central great barrier reef, australia. *Sedimentology*, 31(3):
335–352, 1984.
- [47] P. Johnston. The effect of spatially non-uniform water loads
on prediction of sea-level change. *Geophysical Journal
International*, 114(3):615–634, 1993.
- [48] R. A. Kendall, J. X. Mitrovica, and G. A. Milne. On post-
glacial sea level–ii. numerical formulation and comparative
results on spherically symmetric models. *Geophysical
Journal International*, 161(3):679–706, 2005.
- [49] J. A. Kleypas. *Geological development of fringing reefs in
the Southern Great Barrier Reef, Australia*. James Cook
University of North Queensland, 1991.
- [50] J. A. Kleypas and D. Hopley. Reef development across
a broad continental shelf, southern great barrier reef, aus-
tralia. In *Proc*, volume 7, pages 1129–1141, 1992.
- [51] J. Kuchar, G. Milne, and K. Latychev. The importance of
lateral earth structure for north american glacial isostatic
adjustment. *Earth and Planetary Science Letters*, 512:
236–245, 2019.

- 882 [52] K. Lambeck, A. Purcell, P. Johnston, M. Nakada, and
883 Y. Yokoyama. Water-load definition in the glacio-hydro-
884 isostatic sea-level equation. *Quaternary Science Reviews*,
885 22(2-4):309–318, 2003.
- 886 [53] K. Latychev, J. X. Mitrovica, J. Tromp, M. E. Tamisiea,
887 D. Komatitsch, and C. C. Christara. Glacial isostatic ad-
888 justment on 3-d earth models: a finite-volume formulation.
889 *Geophysical Journal International*, 161(2):421–444, 2005.
- 890 [54] T. Lorscheid and A. Rovere. The indicative meaning
891 calculator–quantification of paleo sea-level relationships
892 by using global wave and tide datasets. *Open Geospatial*
893 *Data, Software and Standards*, 4(1):1–8, 2019.
- 894 [55] J. F. Marshall and P. J. Davies. Last interglacial reef growth
895 beneath modern reefs in the southern great barrier reef.
896 *Nature*, 307(5946):44–46, 1984.
- 897 [56] M. T. McCulloch and T. Esat. The coral record of last inter-
898 glacial sea levels and sea surface temperatures. *Chemical*
899 *Geology*, 169(1-2):107–129, 2000.
- 900 [57] M. McNeil, L. D. Nothdurft, Q. Hua, J. M. Webster, and
901 P. Moss. Evolution of the inter-reef halimeda carbonate
902 factory in response to holocene sea-level and environmen-
903 tal change in the great barrier reef. *Quaternary Science*
904 *Reviews*, 277:107347, 2022.
- 905 [58] G. A. Milne and J. X. Mitrovica. Postglacial sea-level
906 change on a rotating earth: first results from a gravita-
907 tionally self-consistent sea-level equation. *Geophysical*
908 *Journal International*, 126(3):F13–F20, 1996.
- 909 [59] G. A. Milne, J. X. Mitrovica, and J. L. Davis. Near-field
910 hydro-isostasy: the implementation of a revised sea-level
911 equation. *Geophysical Journal International*, 139(2):464–
912 482, 1999.
- 913 [60] J. X. Mitrovica and G. Milne. On the origin of late
914 holocene sea-level highstands within equatorial ocean
915 basins. *Quaternary Science Reviews*, 21(20-22):2179–
916 2190, 2002.
- 917 [61] J. X. Mitrovica and G. A. Milne. On post-glacial sea level:
918 I. general theory. *Geophysical Journal International*, 154
919 (2):253–267, 2003.
- 920 [62] J. X. Mitrovica, J. Wahr, I. Matsuyama, and A. Paulson.
921 The rotational stability of an ice-age earth. *Geophysical*
922 *Journal International*, 161(2):491–506, 2005.
- 923 [63] C. Murray-Wallace and A. Belperio. The last interglacial
924 shoreline in australia—a review. *Quaternary Science Re-*
925 *views*, 10(5):441–461, 1991.
- 926 [64] M. Nakada and K. Lambeck. Late pleistocene and
927 holocene sea-level change; evidence for lateral mantle vis-
928 cosity structure? *Glacial Isostasy, Sea-Level and Mantle*
929 *Rheology*, pages 79–94, 1991.
- 930 [65] M. J. O’Leary, P. J. Hearty, W. G. Thompson, M. E. Raymo,
931 J. X. Mitrovica, and J. M. Webster. Ice sheet collapse
932 following a prolonged period of stable sea level during the
933 last interglacial. *Nature Geoscience*, 6(9):796–800, 2013.
- 934 [66] N. Opdyke, D. Spangler, D. Smith, D. Jones, and
935 R. Lindquist. Origin of the epeirogenic uplift of pliocene-
936 pleistocene beach ridges in florida and development of the
937 florida karst. *Geology*, 12(4):226–228, 1984.
- [67] W. Peltier and R. G. Fairbanks. Global glacial ice volume
and last glacial maximum duration from an extended bar-
bados sea level record. *Quaternary Science Reviews*, 25
(23-24):3322–3337, 2006.
- [68] J. Pickett, C. Thompson, R. Kelley, and D. Roman. Evi-
dence of high sea level during isotope stage 5c in queens-
land, australia. *Quaternary Research*, 24(1):103–114,
1985.
- [69] J. Pickett, T. Ku, C. Thompson, D. Roman, R. Kelley, and
Y. Huang. A review of age determinations on pleistocene
corals in eastern australia. *Quaternary Research*, 31(3):
392–395, 1989.
- [70] T. Pico, J. X. Mitrovica, K. L. Ferrier, and J. Braun. Global
ice volume during mis 3 inferred from a sea-level analy-
sis of sedimentary core records in the yellow river delta.
Quaternary Science Reviews, 152:72–79, 2016.
- [71] M. E. Raymo, J. X. Mitrovica, M. J. O’Leary, R. M.
DeConto, and P. J. Hearty. Departures from eustasy in
pliocene sea-level records. *Nature Geoscience*, 4(5):328–
332, 2011.
- [72] F. D. Richards, M. J. Hoggard, N. White, and S. Ghe-
lichkhan. Quantifying the relationship between short-
wavelength dynamic topography and thermomechanical
structure of the upper mantle using calibrated parame-
terization of anelasticity. *Journal of Geophysical Re-*
search: Solid Earth, 125:e2019JB019062, 2020. doi:
10.1029/2019JB019062.
- [73] F. D. Richards, M. J. Hoggard, S. Ghelichkhan, P. Koele-
meijer, and H. C. Lau. Geodynamic, geodetic, and seismic
constraints favour deflated and dense-cored llvps. *Earth*
and Planetary Science Letters, 602:117964, 2023.
- [74] J. Ritsema, A. Deuss, H. J. Van Heijst, and J. H. Wood-
house. S40RTS: A degree-40 shear-velocity model for
the mantle from new Rayleigh wave dispersion, teleseis-
mic traveltimes and normal-mode splitting function mea-
surements. *Geophysical Journal International*, 184:1223–
1236, 2011. ISSN 0956540X. doi: 10.1111/j.1365-246X.
2010.04884.x.
- [75] A. Rovere, P. Stocchi, and M. Vacchi. Eustatic and relative
sea level changes. *Current Climate Change Reports*, 2(4):
221–231, 2016.
- [76] A. Rovere, T. Pico, F. Richards, M. J. O’Leary, J. X.
Mitrovica, I. D. Goodwin, J. Austermann, and K. Laty-
chev. Supplementary data for: "The influence of reef
isostasy, dynamic topography, and glacial isostatic ad-
justment on the Last Interglacial sea- level record of
Northeastern Australia" (version 1.1), Aug. 2022. URL
<https://doi.org/10.5281/zenodo.7697073>.
- [77] G. A. Ruetenik, K. L. Ferrier, J. R. Creveling, and M. Fox.
Sea-level responses to rapid sediment erosion and deposi-
tion in taiwan. *Earth and Planetary Science Letters*, 538:
116198, 2020.
- [78] E. Ryan, S. Smithers, S. Lewis, T. Clark, J.-X. Zhao, and
Q. Hua. Fringing reef growth over a shallow last inter-
glacial reef foundation at a mid-shelf high island: Hol-
bourne island, central great barrier reef. *Marine Geology*,
398:137–150, 2018.

- 995 [79] A. Sansoleimani, G. E. Webb, D. L. Harris, S. R. Phinn, J. M. Webster and P. J. Davies. Coral variation in two deep
 996 and C. M. Roelfsema. Antecedent topography and active drill cores: significance for the pleistocene development
 997 tectonic controls on holocene reef geomorphology in the of the great barrier reef. *Sedimentary Geology*, 159(1-2):
 998 great barrier reef. *Geomorphology*, 413:108354, 2022. 61–80, 2003. 1054
 999 ISSN 0169-555X. doi: [https://doi.org/10.1016/j.geomorph.](https://doi.org/10.1016/j.geomorph.2022.108354)
 1000 2022.108354. URL [https://www.sciencedirect.](https://www.sciencedirect.com/science/article/pii/S0169555X22002471)
 1001 [com/science/article/pii/S0169555X22002471](https://www.sciencedirect.com/science/article/pii/S0169555X22002471).
- 1002 [80] A. J. Schaeffer and S. Lebedev. Global shear speed struc-
 1003 ture of the upper mantle and transition zone. *Geophys- 1055*
 1004 ical Journal International, 194:417–449, 2013. ISSN 1056
 1005 0956540X. doi: 10.1093/gji/ggt095.
- 1006 [81] I. Shennan, A. J. Long, and B. P. Horton. *Handbook of 1057*
 1007 *sea-level research*. John Wiley & Sons, 2015. 1058
- 1008 [82] N. Simmons, S. Myers, G. Johannesson, E. Matzel, and 1059
 1009 S. Grand. Evidence for long-lived subduction of an 1060
 1010 ancient tectonic plate beneath the southern Indian Ocean. *Journal of Geophysical 1061*
 1011 *Research Letters*, 42(21):9270–9278, 2015. 1062
- 1012 [83] M. Spalding, M. D. Spalding, C. Ravilius, and E. P. Green. 1063
 1013 *World atlas of coral reefs*. Univ of California Press, 2001. 1064
- 1014 [84] B. Steinberger, S. C. Werner, and T. H. Torsvik. Deep 1065
 1015 versus shallow origin of gravity anomalies, topography 1066
 1016 and volcanism on Earth, Venus and Mars. *Icarus*, 207(2): 1067
 1017 564–577, 2010. 1068
- 1018 [85] S. N. Stephenson, N. J. White, T. Li, and L. F. Robinson. 1069
 1019 Disentangling interglacial sea level and global dynamic 1070
 1020 topography: Analysis of madagascar. *Earth and Planetary 1071*
 1021 *Science Letters*, 519:61–69, 2019.
- 1022 [86] S. N. Stephenson, N. White, A. Carter, D. Seward, P. Ball, 1069
 1023 and M. Klöcking. Cenozoic dynamic topography of mada- 1070
 1024 gascar. *Geochemistry, Geophysics, Geosystems*, 22(6): 1071
 1025 e2020GC009624, 2021.
- 1026 [87] C. Stirling, T. Esat, K. Lambeck, and M. McCulloch. Tim-
 1027 ing and duration of the last interglacial: evidence for a
 1028 restricted interval of widespread coral reef growth. *Earth 1069*
 1029 *and Planetary Science Letters*, 160(3-4):745–762, 1998. 1070
- 1030 [88] UNEP-WCMC, WorldFish Centre, WRI, TNC. Global
 1031 distribution of warm-water coral reefs, compiled from mul-
 1032 tiple sources including the millennium coral reef mapping
 1033 project. version 4.0, 2010. [http://data.unep-wcmc.](http://data.unep-wcmc.org/datasets/1)
 1034 [org/datasets/1](http://data.unep-wcmc.org/datasets/1).
- 1035 [89] O. Van de Plassche. *Sea-level research: A manual for the 1069*
 1036 collection and evaluation of data: Norwich. UK, *Geobooks,* 1070
 1037 1986. 1071
- 1038 [90] C. Waelbroeck, L. Labeyrie, E. Michel, J.-C. Duplessy, J. F.
 1039 Mcmanus, K. Lambeck, E. Balbon, and M. Labracherie.
 1040 Sea-level and deep water temperature changes derived
 1041 from benthic foraminifera isotopic records. *Quaternary 1069*
 1042 *science reviews*, 21(1-3):295–305, 2002. 1070
- 1043 [91] R. Walker, M. Telfer, R. Kahle, M. Dee, B. Kahle, J.-L.
 1044 Schwenninger, R. Sloan, and A. Watts. Rapid mantle-
 1045 driven uplift along the angolan margin in the late quater-
 1046 nary. *Nature Geoscience*, 9(12):909–914, 2016. 1071
- 1047 [92] J. X. W. Wan, N. Gomez, K. Latychev, and H. K. Han.
 1048 Resolving glacial isostatic adjustment (gia) in response to
 1049 modern and future ice loss at marine grounding lines in
 1050 west antarctica. *The Cryosphere*, 16(6):2203–2223, 2022.